Facultad de Ciencias
Universidad de Cantabria

Search for dark matter production in association with top quarks in the dilepton final state at $\sqrt{s} = 13$ TeV

A thesis submitted in fulfillment of the requirements for the

Degree of Doctor of Philosophy

Written by

Cédric Prieëls

Under the supervision of

Jónatan Piedra Gómez
Pablo Martínez Ruiz del Árbol

Santander, June 2020

Abstract

Resumen

Acknowledgments

Acronyms used

SM Standard Model

DM Dark Matter

LHC Large Hadron Collider

CMS Compact Muon Solenoid

ATLAS A Toroidal LHC ApparatuS

CERN European Council for Nuclear Research

QFT Quantum Field Theory

CMB Cosmic Microwave Background

ML Machine Learning

MFV Minimal Flavour Violation

WIMP Weakly Interactive Massive Particle

PF Particle Flow

BSM Beyond the Standard Model

MACHO Massive Compact Halo Object

MSSM Minimal Supersymmetric Standard Model

SI Spin Independent

SD Spin Dependent

CL Confidence Level

QCD Quantum ChromoDynamics

ADMX Axion Dark Matter Experiment

CAST CERN Axion Solar Telescope

IAXO International Axion Observatory

LNGS Laboratori Nazionali del Gran Sasso

UED Universal Extra Dimensions

NFW Navarro-Frenk-White

LAT Fermi Large Telescope

IACT Imaging Atmospheric Cherenkov Telescopes

CTA Cherenkov Telescope Array

AMS Alpha Magnetic Spectrometer

EFT Effective Field Theory

ISR Initial State Radiation

DMWG Dark Matter Working Group

MET Missing Transverse Energy

VBF Vector Boson Fusion

BR Branching Ratio

LEP Large Electron Positron collider

ALICE A Large Ion Collider Experiment

PS Proton Synchrotron

SPS Super Proton Synchrotron

PU Pile Up

PV Primary Vertex

ECAL Electromagnetic Calorimeter

HCAL Hadronic Calorimeter

DT Drift tube

CSC Cathode Strip Chamber

RPC Resistive Plate Chamber

TIB/TBD Tracker Inner Barrel and Disks

TOB Tracker Outer Barrel

TEC Tracker EndCap

HO Hadron Outer

LS Long Shutdown

GEM Gas Electron Multiplier

L1 Level-1 Trigger

HLT High-Level Trigger

DAQ Data Acquisition System

DQM Data Quality Monitoring

DCS Detector Control System

WP Working Point

SC Super Cluster

KF Kalman Filter

GSF Gaussian Sum Filter

MVA Multi-Variate Analysis

CSV Combined Secondary Vertex

DNN Deep Neural Network

PUPPI Pileup Per Particle Identification

BW Breit-Wigner

MC Monte Carlo

UE Underlying Event

PDF Parton Density Function

LO Leading Order

NLO Next to Leading Order

Contents

Chapter 1

Objects reconstruction

As we just saw, the Compact Muon Solenoid (CMS) detector is made out of different layers, each able to convert the interaction of the particle with this detector into electronic signals that can be measured and stored. However, this signal collected is made out of raw information coming from different kind of sub-systems and an algorithmic strategy then needs to be put in place in order to read all these separate signals and to combine them to extract some useful data, such as the number of particles produced by the collision along with their energy, charge and direction. Producing this kind of data is essential for all the offline analyses which usually rely on these high-level physics objects to make precision measurements or search for new physics.

The algorithm able to combine this raw data and to produce useful objects and variables is the so-called Particle Flow (PF) algorithm [89], which will be described in Section 1.1. Then, a particular focus will be given to the definition and reconstruction of different objects of our particular analysis, such as the electrons and muons (Section 1.3), the jets (Section 1.4), the Missing Transverse Energy (MET) (Section 1.5) and the top reconstruction (Section 1.6) of the different *pp* collisions recorded.

1.1 Particle Flow (PF) algorithm

The Particle Flow (PF) is an algorithm aiming to combine in the best way possible all the information coming from the different parts of the CMS detector in order to identify and reconstruct the hundreds of new particles produced by each *pp* collision provided by the Large Hadron Collider (LHC). This reconstruction can be divided into two main steps: first of all, the data coming from the different sub-systems of the detector is read in order to identify and measure the properties of some basic stable objects, such as leptons, photos and hadrons. Then, more complex calculations are performed to identify eventual unstable particles, jets from the hadronization of quarks and to compute complex variables such as the leptons isolation and the Missing Transverse Energy (MET).

The most basic elements used by this algorithm for the reconstruction of high-level physics objects are the tracks of charged particles, the clusters of energy left in the two calorimeters and the hits recorded in the muon chambers. For this algorithm to be as efficient as possible, the detector has

been carefully designed: a magnetic field as large as possible and a small calorimeter granularity are indeed crucial in order to separate efficiently charged and neutral particles, and the tracker was designed to be as efficient and small as possible to have the smallest material budget possible in front of the calorimeters.

The way the different particles produced in each collision are identified is quite easy to summarize and is represented in Figure 1.1. Basically, the different kind of particles produced are going to interact with different parts of the detector and combining the information given by the tracker and the rest of the sub-systems then allows to unequivocally identify each particle. This is usually done in a specific order in order to be as efficient as possible:

1. First of all, the most energetic **Primary Vertex (PV)** is identified by taking into account the Pile Up (PU) and by assigning the different tracks to the different pp collisions happening during a single bunch-crossing.

   All the particles originating from less energetic PV or from a secondary vertex of interaction are typically ignored and the corresponding hits in the tracker left by such particles can therefore be removed, leaving less hits available for the clustering algorithm later on, allowing for a more efficient reconstruction of the following objects.

2. Then, **muons** are the easiest particles to identify since they are at first order the only particles leaving many hits in the muon chambers placed on the outside of the detector. Each muon identified is associated to its track in the tracker, where all the hits matching a muon can therefore be removed.

3. **Electrons** do have a charge, so they are visible by the tracker and by the Electromagnetic Calorimeter (ECAL), where they are going to produce an electromagnetic shower. Identifying electrons is a bit more challening than muons because of their associated bremsstrahlung emission of photons that need to be attached to the original electrons to avoid any double counting. All the tracker hits corresponding to electrons are also removed after identification.

4. **Charged hadrons** also leave hits in the tracker and some energy deposits in the ECAL, but mostly in the Hadronic Calorimeter (HCAL), so they are easy to identify as well as a third step, using the latest hits available in the tracker.

5. **Photons** are on the other hand neutral particles, so they do not lave any hits in the tracker. They then appear as some energy deposits in the ECAL for which no corresponding tracker track can be associated.

6. Finally, **neutral hadrons** can be identified as particles leaving some energy mostly in the HCAL for which no corresponding tracker track has been found as well.

We will now study in a bit more details the reconstruction method applied in order to reconstruct the main objects of this analysis, i.e. leptons, jets, MET and top quarks.

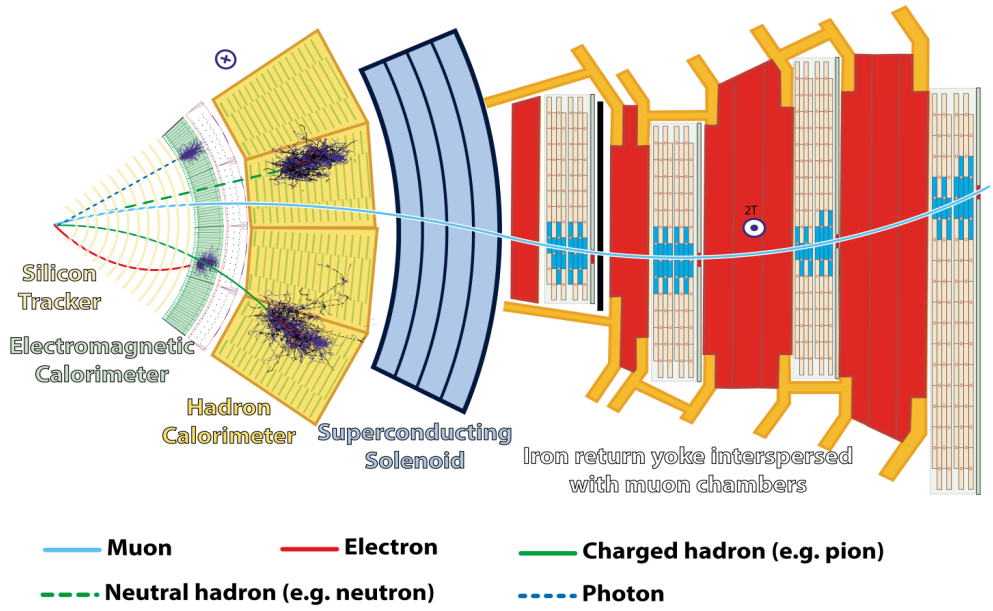

Figure 1.1: Transverse section of CMS showing the different tracks expected by different kind of particles in the detector.

1.2 Primary Vertex (PV) definition

Different kind of vertices originating from a single pp collision can usually be defined, as shown in Figure 1.2: the **Pile Up (PU) vertices**, corresponding to the different simultaneous collisions of a single bunch-crossing of the LHC, the **primary vertex**, usually assumed to be the most energetic PU vertex and the only vertex considered in most of the physics analyses, and the **secondary vertices**, due to the eventual presence of long lived particles, decay chains or jets.

The first task of the PF algorithm is to identify all these vertices of the interaction. This is done by considering all the tracker tracks, by clustering them together and by performing fits to determine the likelihood these tracks originated from a common vertex. The reconstructed vertex with the largest total p_T is then assumed to be the PV, as it is considered to be the origin of the most interesting pp collision from which many different tracks are emitted.

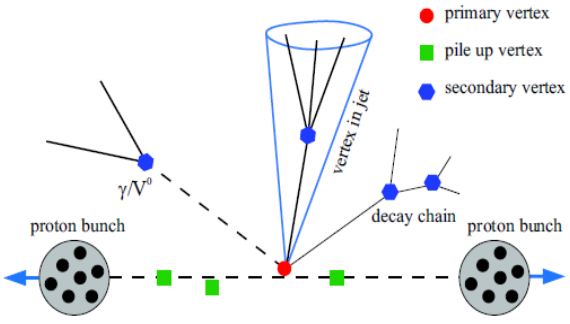

Figure 1.2: Different kind of vertices typically observed in a pp collision in the LHC.

1.3 Leptons reconstruction

Different kind of leptons are typically produced by a pp collision. The muons and the electrons can be quite easily identified, mainly because their lifetime and velocity is high enough, meaning that they are not expected to decay inside the CMS detector, so they can be directly identified. Taus on the other hand are a bit trickier to deal with because they usually decay inside of the beam pipe itself, $\sim 35\%$ of the time to electrons and muons and $\sim 65\%$ of the time to hadrons. However, since our analysis does not consider taus directly but only the leptons originating from the their decays, the details of their reconstruction will not be explained in this section.

1.3.1 Muons

Muons are the first leptons to be reconstructed by the PF algorithm since, at first order, they are the only particles expected to reach the muon chambers, resulting in their easy identification.

The typical signature of a muon consists in several hits in the silicon tracker forming a track since muons do have an electric charge, associated with several hits in the muon chambers, electronic signals coming from the wires and strips of these chambers due to the gas ionization induced by the passage of these charged particles. Muons only deposit a negligible amount of energy within the two calorimeters since their interaction cross section is quite low for their full range of energies, going from a few hundreds MeV up to a few TeV.

The data coming from the different sub-systems of CMS are then combined and fed into three different PF algorithms, able to reconstruct different kind of muons.

Standalone muons

These are muons reconstructed using only the hits observed in the muon system without trying to relate this data to the tracker hits. Basically, the PF algorithm looks in this case at the eventual hits left in the Drift tubes (DTs), Cathode Strip Chambers (CSCs) and Resistive Plate Chambers (RPCs) and tries to reconstruct a vector of trajectory in each case using a Kalman Filter (KF) filter [90]. These segments are then combined in the best statistical way possible in order to form a candidate track for each muon of the event, by extrapolating the innermost vectors are propagated to the layer surface of the next chamber and by comparing it with the local track segment. The trajectory parameters are then computed and the process continues until reaching the outermost chamber, before being reversed in order to estimate the innermost track parameters as well.

To limit the possibility of misidentification due to showering of cosmic rays, the tracks need to pass some quality criteria in order to be considered valid: for example, at least two hits need to be measured for the fit to be performed, one of them coming from either the DTs or CSCs, in order to remove fake segments contamination due to combinatories. Additional constraints by checking the extrapolation of the trajectory to the point of closest approach to the beam line also

allow to reduce this contamination.

Candidates reconstructed as standalone muons typically have a worse momentum reconstruction and are more sensitive to cosmic muons contamination.

Tracker muons

The algorithm able to reconstruct such muons on the other hand is able to propagate tracks identified in the inner silicon tracker (having a momentum $p > 2.5$ GeV and $p_T > 0.5$ GeV) to the muon system itself in order to try and find corresponding segments in the different muon chambers (these tracks are therefore said to be built *inside-out*).

These muons are particularly efficient for less instrumented regions of the detector and for the low p_T end of the energy spectrum but they are also quite contaminated with fake muons tracks, since a single hit in any of the muon chambers is enough for the candidate to be considered a valid tracker muon, even though hadron shower remnants can for example quite easily reach the innermost muon station. The momentum assigned to such muons is the same as the one measured by the silicon tracker track itself.

Global muons

Finally, these muons are built *outside-in* since they are obtained matching standalone muon tracks with independently reconstructed tracks coming from the tracker itself (of course, in order to avoid any double counting, global muons and tracker muons that share the same tracker track are actually merged into a single candidate).

This category of muons presents the advantage of being less sensitive to the muon misidentification rate than tracker muons since it uses the information from more than one muon chamber. The p_T measurement in this case is also improved (especially at high p_T, > 200 GeV) by exploiting the information from both the inner tracker and the muon system, while at low momentum, the best momentum resolution for muons is obtained from the inner silicon tracker directly.

Using this strategy, about 99% of the muons produced within the geometrical acceptance of the muon system are reconstructed either as global or tracker muons [88], as seen in Figure 1.3.

Once reconstructed, candidates are required to pass some selection criteria and are then fed to the actual PF algorithm itself to start the global reconstruction of the event. This selection consists mainly in applying identification and isolation (evaluated relative to its p_T by summing up the energy in geometrical cones of radius $\Delta R = \sqrt{(\Delta\phi)^2 + (\Delta\eta)^2}$ surrounding the muon, as shown in Figure 1.4) criteria in order to enhance the purity of the reconstructed muons by rejecting muons coming from W+jets and QCD processes.

Different Working Points (WPs) can then be defined for the offline analyses, from loose to tight, in order to reject more or less contamination from misidentified leptons, keeping in mind that a tighter selection will also have an impact on the efficiency of the selection. The actual selection applied to the global muons used in this particular analysis will be detailed in Chapter 3.

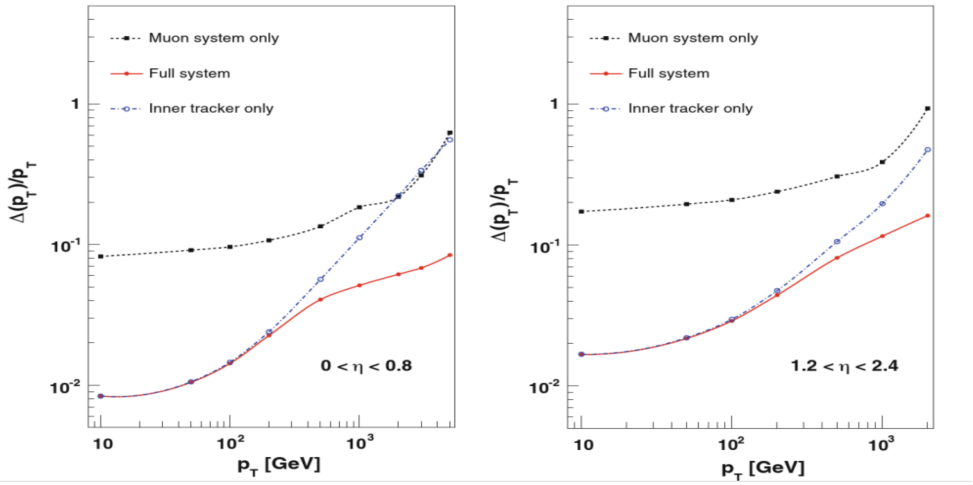

Figure 1.3: Muon p_T resolution obtained in simulation in the barrel (on the left) and endcap (on the right) for different kind of reconstructed muons [91].

1.3.2 Electrons

Electrons are reconstructed by combining the tracker tracks and the several clusters of energy deposited in the ECAL by the electromagnetic showers appearing due to the interaction between the electron and the crystals composing this sub-detector.

It is usually a bit harder to reconstruct electrons than muons mainly because electrons do interact with the tracker and this interaction therefore needs to be modeled to understand the exact behaviour of such particles: this interaction is for example responsible for the emission of secondary bremsstrahlung photons crashing into the ECAL but not coming from the PV. In fact, it is estimated that in CMS between 33% and 86% of the energy of an electron is actually radiated before it reaches the ECAL, depending mostly on its pseudorapidity [92]. In order to measure precisely the energy of an electron, all the photons emitted by bremsstrahlung before reaching the ECAL (usually, along the ϕ axis because of the deviation implied by the solenoid) then need to be collected as well and associated to the correct electron of the event.

The actual PF reconstruction of electrons is performed in different steps:

1. A **clustering algorithm** is first of all defining the so-called **Super Cluster (SC)**. Its goal is to reconstruct the particle showers individually by identifying a seed crystal for the cluster, defined as the crystal collecting the most energy, since the energy deposited in the ECAL is usually spread into several different crystals because of the electromagnetic shower effect discussed in Section **??** and because of the bremsstrahlung emission of photons due to the interaction with the tracker. The algorithm therefore searches for eventual crystals around this seed whose energy detected would be superior to 2σ of the electronic noise and matching some quality criteria ($E_{\text{seed}} > 230$ MeV in the barrel, $E_{\text{seed}} > 600$ MeV and $E^T_{\text{seed}} > 150$ MeV in the endcaps).

   The excited contiguous crystals found are then grouped into clusters, themselves considered candidates for the final global cluster, the SC, if their energy is higher than another given

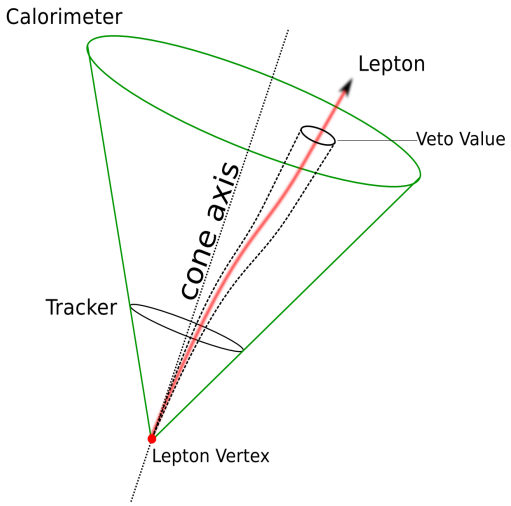

Figure 1.4: Lepton isolation cone typically used to reduce the background levels from Standard Model (SM) processes.

threshold ($E_{\text{cluster}} > 350$ MeV in the barrel, $E^{T}_{\text{cluster}} > 1$ GeV in the endcaps) [92]. The SC energy is then given by the sum of the energies of all its constituent clusters, while its position is calculated as the energy-weighted mean position of the different clusters.

2. Once the SC identified, **electron tracker tracks** are reconstructed using a procedure a bit different than the usual KF reconstruction method for all the tracks of the silicon tracker [90] because of the large radiative losses for electrons in the tracker material.

   This reconstruction is known to be very time consuming, so a good identification of potential electron seeds has to be performed as the method efficiency greatly relies on this first identification. Two different strategies can be used to perform this seeding (even though the electron seeds found using the two algorithms are usually combined afterwards):

   - The **ECAL-based seeding** relies on the information obtained for the SC energy and position in order to estimate the electron trajectory to find compatible hits in the tracker. This can be done knowing that the electron or positron is moving according to an helix in the magnetic field of the detector. This seeding is mostly optimized for isolated electron in the p_T range relevant for the Z and W decays.
   - The other way to proceed is the **tracker-based seeding**, based on tracks reconstructed using the usual KF algorithm and looking for matches within the possible reconstructed SC. This seeding is mostly suitable for low p_T electrons and also performs quite well with electrons inside jets.

   Once the seeds identified, the identification of tracks can begin. First of all, the gathering of compatible of hits from the different seeds is done using using a dedicated modeling of the electron energy loss and a combinatorial KF algorithm allowing to construct possible tracks when compatible hits are found. The compatibility matching between the predicted and found hits is usually chosen to be quite loose in order to maintain a good efficiency even in case of bremsstrahlung emission.

Finally, once the hits are collected, a Gaussian Sum Filter (GSF) fit is performed to estimate the different track parameters by reconstructing the layer-to-layer propagation of electrons in the tracker. A mix of Gaussian distributions is used in this case to approximate the loss in each layer, associating a different weight and χ^2 penalty to each distribution, depending for example on the number of missing hits. This fit is also able to take into account sudden changes in the curvature radius caused by an eventual bremsstrahlung photon emission.

3. The final step consists in identifying the clusters left in the ECAL by the photons emitted by extrapolation of the GSF track and in **merging this GSF track and the ECAL SCs** previously built. This step is also designed to preserve the highest efficiency possible while keeping the misidentification probability low and ambiguities related to single electron seeds which can often lead to several reconstructed tracks are also resolved at this stage.

   Finally, a loose preselection is applied to the electron candidates in order to reject fake electrons and the variables related to the energy and geometrical matching between the GSF track and the ECAL cluster(s) are combined into a Multi-Variate Analysis (MVA) estimator allowing to define several electron Working Point (WP) as well.

This complete electron workflow explained here in a simplified way can be summarized in Figure 1.5.

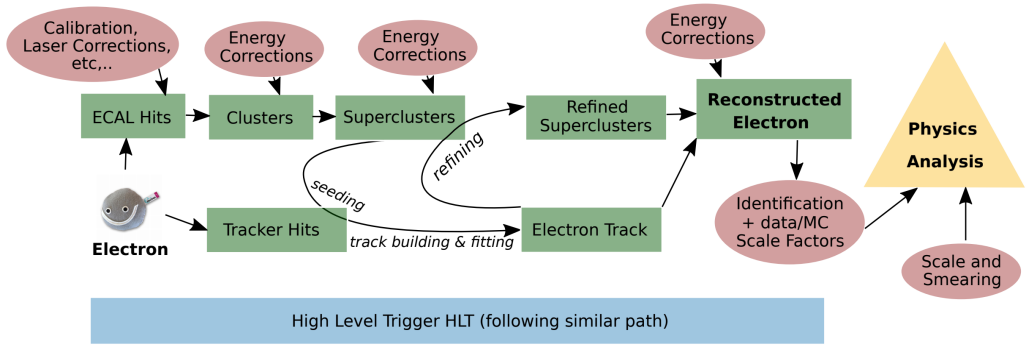

Figure 1.5: Schematic representation of the full electron reconstruction workflow in CMS [93].

1.4 Jets reconstruction

Eventual jets and gluons produced by a *pp* collision of the LHC usually manifest themselves as hadronic jets in the detector because of the colour confinment principle stating that coloured particles, such as the quarks, cannot be isolated and therefore be observed on their own.

This practically means that once a single quark is produced, it will start losing energy by forming new $q\bar{q}$ pairs, themselves forming additional $q\bar{q}$ pairs. This chain continues until the resulting pairs of quarks have such a low energy that they can start combining into colourless hadrons. This is called the *hadronization* process and the actual result of the apparition of a quark is a shower of collimated particles, usually called jet, and seen by the detector as a set of tracks and energy deposits in the calorimeters, as shown in Figure 1.6.

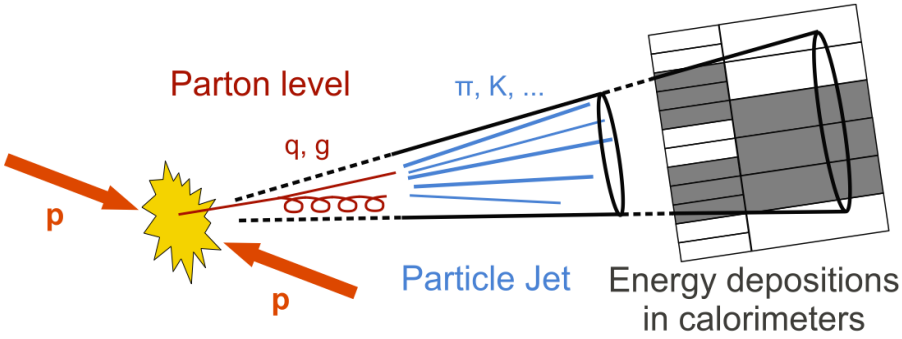

Figure 1.6: Schematic representation of the typical development of a jet within the CMS detector.

Several algorithms can be used to reconstruct the jets by linking the information coming from the tracker and the calorimeters, but the most used tool in CMS is the so-called anti-k_T algorithm, able to cluster all the charged and neutral hadrons along with the eventual non-isolated photons or lepton produced and merge them into a single jet [94]. Its main objective is to compute the energy and direction of the original quark as precisely as possible. This is actually the best algorithm developed so far to resolve jets, but the worst for studying jet substructure due to its clustering preference.

To perform such a job, sequential clustering algorithm such as this one rely on the value of two distances: d_{ij}, the distance between two particles i and j that need to be clustered and d_{iB}, the distance between the particle i and the beam axis B. As seen in Equation 1.1, these distances can be computed using different variables such as $\Delta R_{ij}^2 = (\eta_i - \eta_j)^2 + (\phi_i + \phi_j)^2$, the distance between i and j in the $(\eta - \phi)$ space, the p_T^2 of each particle and R^2, the algorithm radius parameters determining the final jet size and usually set to 0.4 by the CMS collaboration.

$$\begin{cases} d_{ij} = \min\left(\frac{1}{p_{T,i}^2}, \frac{1}{p_{T,j}^2}\right) \frac{\Delta R_{ij}^2}{R^2} \\ d_{iB} = \frac{1}{p_{T,i}^2} \end{cases} \tag{1.1}$$

The algorithm works by looking at all the i, j combinations, comparing the distances d_{ij} and d_{iB} until only jets are present in the event:

- If d_{ij} is smaller, then i and j are combined into a single particle (ij) by summing their 4-vectors and both are removed from the list of particles to be clustered.
- If d_{iB} is smaller, then i is considered to be the final jet and is therefore removed from the list of jet candidates as well.

Several corrections are then usually applied to the jets constructed using this algorithm, in order to take into account several parameters, such as the non-linearity of the response of the calorimeter, the electronic noise, the Pile Up (PU) effects and the dependance of the reconstruction on the jet flavor and distance parameter R. This typically introduces a source of uncertainty that will be taken into account and discussed in Section 4.1.

The efficiency of the PF algorithm for jet identification and reconstruction has been checked using simulation, as shown in Figure 1.7. This study clearly shows that between 95 and 97% of the energy of the PF jet candidates can be reconstructed, compared to a 40-60% reconstruction efficiency using only the calorimeters data, and that this algorithm also leads to a gain in resolution up to a factor 3, depending on the jet p_T.

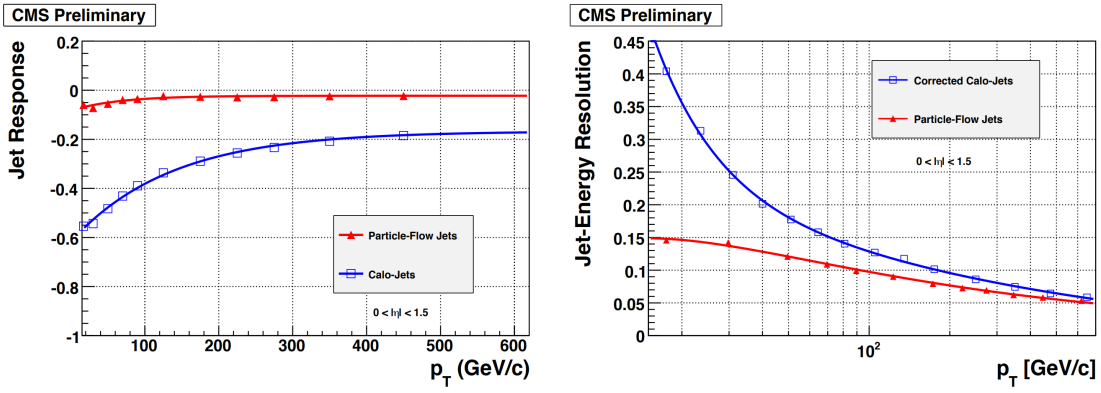

Figure 1.7: Comparison of the jet response (on the left) and jet energy resolution (on the right) for dijets simulated events in the barrel for jets reconstructed using only the calorimeters (in blue) and jet candidates from the PF algorithm (in red) [96].

1.4.1 B-tagging

Jets coming from bottom quarks are usually quite interesting to study, especially in this analysis which relies heavily on the number of b-jets produced to define the control and signal regions, as will be discussed in Chapter 3.

This specific kind of jets can be distinguished from other jets because of the relatively long lifetime of the bottom quark ($\tau \sim 1.5$ ps) that produces in the detector a secondary vertex displaced by a few millimeters with respect to the PV, as shown in Figure 1.8; and this gives a perfect way to discriminate jets coming from light quarks from b-jets. Another consequence of the large mass of the bottom quark is that a large number of particles is typically present inside this particular kind of jets and that the decay of the bottom quark even leads to the apparition of soft leptons in the decay chain in around 20% of the cases.

Because of these specific properties, an algorithm can quite easily distinguish between jets coming from a bottom quark or from a lighter quark, and this will be a key point in this analysis. In our case, this discrimination is additionally optimized by using a multivariate technique able to combine all the discriminating power of the previous typical characteristics of any heavy flavour jet in the best way possible after reconstruction of all the vertices of the event. The main objective of the algorithm is to be able to identify b-jets as efficiently as possible while reducing the risk of possible misidentification of a jet.

In this analysis, the typical deep Combined Secondary Vertex (CSV) algorithm able to combine the information on the secondary vertex with the one on the track impact parameters and based on a Deep Neural Network (DNN) previously trained, has been used to identify such b-jets. The

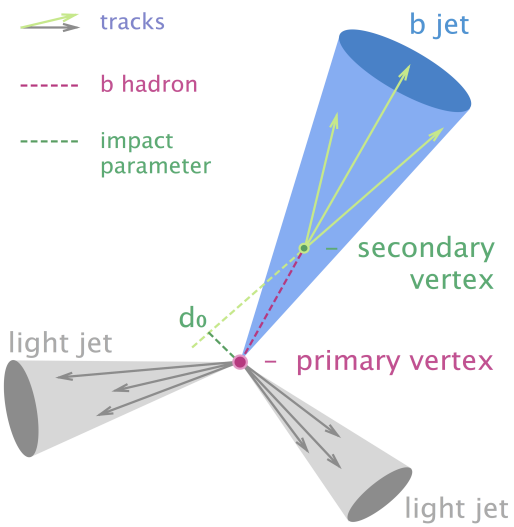

Figure 1.8: Schematic representation of the production of a b-jet originating from a slightly displaced secondary vertex.

performance of this method can be observed in Figure 1.9, where we can see that this deep CSV algorithm is one of the best algorithms able to identify b-jets, depending on the phase space, while keeping a relatively low misidentification rate for light-flavor jets (u, d, s and gluons).

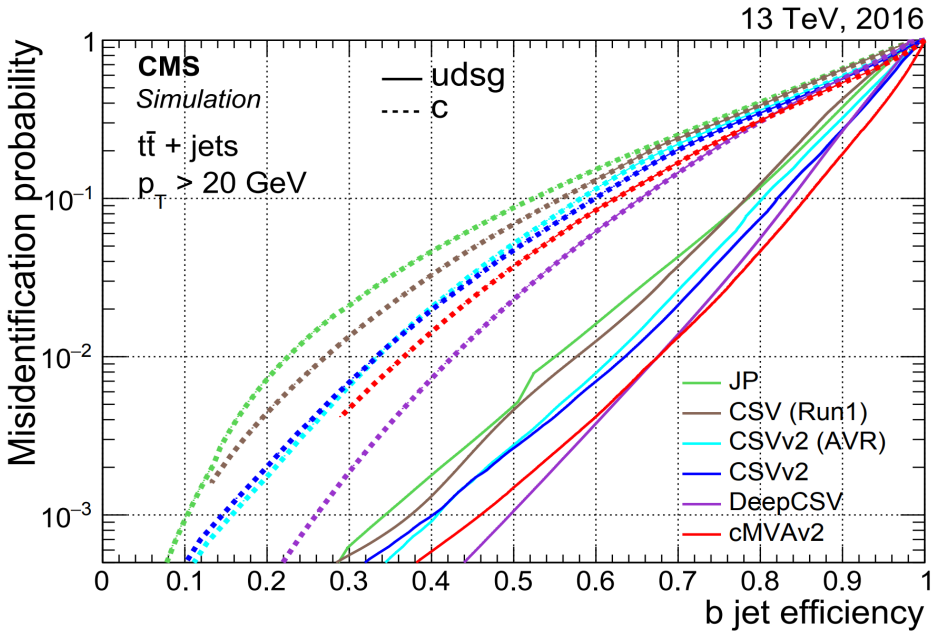

Figure 1.9: B-jets identification efficiency and misidentification rate considering different b-taggers, including the deep CSV b-tag used in this analysis [97].

Different Working Points (WPs) are then made available for all the offline analyses in order to tweak the combo b-jet identification efficiency/misidentification rate. The loose, medium and tight WPs have been developed in such a way to limit this misidentification rate of a light jet as a b-jet to 10%, 1% and 0.1% respectively.

1.5 Missing Transverse Energy (MET)

Since the *pp* collisions happen mostly head-on, we know that the initial total transverse momentum of the event is exactly equal to 0 before the collision and we expect that it stays 0 afterwards because of the momentum conversation.

However, this statement is not totally true since we are aware of several effects that could induce an imbalance in this transverse momentum, as shown in Figure 1.10:

- Even though the detector has been carefully designed, some particles could be created outside of the acceptance of the detector and therefore escape the detection (a particle can for example be created with such a boost that it could be emitted back to the beam pipe itself, making it impossible to detect it).
- Because of their extremely low interaction cross-section, SM neutrinos are expected to escape the detector with some energy staying completely undetected.
- The finite momentum resolution of the detector can also lead to some inaccuracies in the measurement of the transverse momentum of all the particles created, leading to an instrumental MET in some cases.
- Finally, the eventual exotic weakly interacting particles produced, such as Dark Matter (DM), is typically expected to leave some MET in the detector as well.

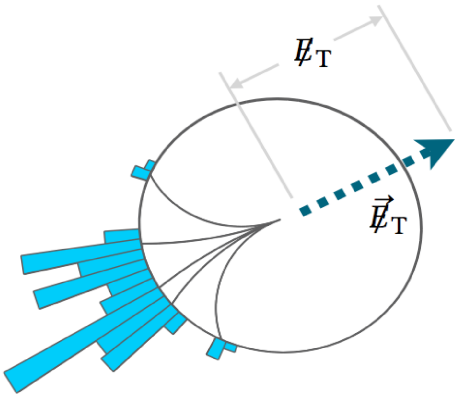

Figure 1.10: Schematic representation of the Missing Transverse Energy (MET).

The Missing Transverse Energy (MET) variable, defined in Equation 1.2 as the negative sum of the transverse momentum of all the particles j of the event, is able to take into account this eventual imbalance in the transverse momentum and is therefore a key variable in most of the analyses searching for new Beyond the Standard Model (BSM) physics, which is not expected to interact with the detector.

$$\vec{p}_T^{\,\text{miss}} = -\sum_j \vec{p}_{T,j} \tag{1.2}$$

Different algorithms can be used in order to reconstruct this variable, the most famous being [98]:

- The **particle flow MET** (PFMET), including all the information of the detector (as opposed to the **calorimeter** or **tracker MET**, for example) and only the PF reconstructed objects to estimate the MET value. This is the typical variable used in most of the analyses today, because of its simple, robust, yet very performant estimate of the MET spectrum.
- The **Pileup Per Particle Identification (PUPPI) MET**, actually used in this analysis, has been developed on top of the PFMET in order to further reduce the dependence on the pileup of this variable by using local shape information around each PF candidate in the event along with event PU properties and tracking information.

Several corrections also need to be applied to this spectrum to filter anomalous high MET events arising because of a variety of reconstruction failures induced by the detector, because of several effects, such as the the electronic noise and eventual dead cells in the calorimeters or the presence of eventual beam halo particles from the LHC itself, leading to a global miscalculation of the final energy of the event. These filters are extremely important, especially in the end of the MET spectrum, as observed in Figure 1.11.

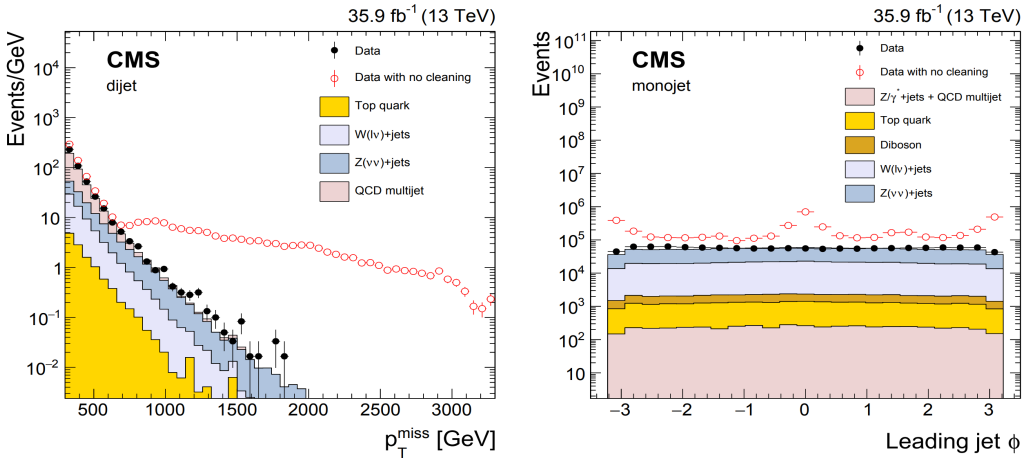

Figure 1.11: MET and jet ϕ distributions with and without MET filters applied [98].

1.6 Top reconstruction

Although not formerly a part of the PF algorithm and done off-line, the kinematic reconstruction of the SM $t\bar{t}$ process represented in Figure 1.12 is still an extremely important part of this analysis. As previously explained, because of the high mass of the top quark, it is expected to decay before reaching the detector, almost 100% of the time into a $b\bar{b}$ pair of quarks, which can be identified using the b-tagging method explained in Section 1.4.1, and a W boson, unstable as well (in our particular case, only the W decay to a lepton and a neutrino is considered for reasons explained in Section **??**, even though this decay has a low Branching Ratio (BR)).

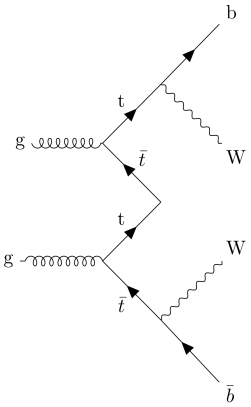

Figure 1.12: Feynman diagram of the SM $t\bar{t}$ production and subsequent decays.

The ideal kinematics of such an event can be expressed using the four-momenta of the different particles involved, as expressed in the Equations 1.3a to 1.3c.

$$\begin{cases} p_x^{\text{miss}} = p_{\nu_x} + p_{\bar{\nu}_x} \\ p_y^{\text{miss}} = p_{\nu_y} + p_{\bar{\nu}_y} \end{cases} \tag{1.3a}$$

$$\begin{cases} m_{W^+}^2 = (E_{l^+} + E_\nu)^2 - (\overrightarrow{p}_{l^+} + \overrightarrow{p}_\nu)^2 \\ m_{W^-}^2 = (E_{l^-} + E_{\bar{\nu}})^2 - (\overrightarrow{p}_{l^-} + \overrightarrow{p}_{\bar{\nu}})^2 \end{cases} \tag{1.3b}$$

$$\begin{cases} m_t^2 = (E_b + E_{l^+} + E_\nu)^2 - (\overrightarrow{p}_b + \overrightarrow{p}_{l^+} + \overrightarrow{p}_\nu)^2 \\ m_{\bar{t}}^2 = (E_{\bar{b}} + E_{l^-} + E_{\bar{\nu}})^2 - (\overrightarrow{p}_{\bar{b}} + \overrightarrow{p}_{l^-} + \overrightarrow{p}_{\bar{\nu}})^2 \end{cases} \tag{1.3c}$$

In all these previous equations, the quantities related to the leptons and the b-jets can be measured using the PF reconstruction, while the energy of the neutrinos can be considered equal to their momentum because of their extremely low mass. It is also important to note that the different masses appearing in these equations will be treated as exactly known even though this is only true at first approximation since they are actually Breit-Wigner (BW) distributions.

We therefore have 6 equations to solve and exactly 6 unknowns corresponding to the three momentum components of each neutrino produced, a problem that can in principle be solved, leading to a quartic equation in one of the unknowns analytically solvable but quite ambiguous given the variable number of solutions of such equation [99].

1.6.1 Top reconstruction in practice

Even though the equations and the problem seems quite well defined and solvable, in practice, several complications quickly appears. First of all, when considering real data, the pairing between the leptons and the b-jets observed is not obvious to perform. Typically, three cases will then be

defined in order to take this effect into account:

- If exactly 0 b-jets are observed, the event will not be considered in this analysis, according to the selection of the signal regions performed and explained later in Chapter 3.
- If more than one b-jet is observed, then only two different permutations considering the two b-jets and the two leptons having the highest momentum $\{l^+ \leftrightarrow b_1, l^- \leftrightarrow b_2\}$ and $\{l^- \leftrightarrow b_1, l^+ \leftrightarrow b_2\}$ are considered.
- Finally, if exactly one b-jet is observed, then it will be kept and all the non b-tagged jets will be considered as the second b-jet candidate. In this case, several combinations between the two leptons and all these jets are then considered, resulting in $2n$ different combinations, where n is the number of jets in the event.

The combination leading to the lowest invariant mass for the $t\bar{t}$ system is then chosen between all the different possibilities for the reconstruction of the system.

Section to be updated once the analysis performed and the details about the top reco performed known, and add the results obtained.

Chapter 2

Data, signals and backgrounds

In order to find a possible hint of the production of DM in the LHC collisions considering our signal models of interest, briefly described in Section **??**, the data collected needs to be compared with Monte Carlo (MC) simulations produced in a central way for each SM process and mathematically able to simulate what is expected to be seen by the detector, taking into account the effect of the detector on the particles produced. This MC production method will be first of all briefly introduced in Section 2.1.

The different data samples collected during the Run II of operation of the LHC will be then detailed in Section 2.2, while the signal models and samples considered in this particular analysis and the MC samples used for the simulation of the different backgrounds will be introduced in Sections 2.3 and **??** respectively.

2.1 The Monte Carlo (MC) simulation method

The production and simulation of samples is a crucial step since most of the analyses performed at the LHC heavily depend on this MC generation to define the signal and background samples that can be directly compared with the data collected, in order to try and find eventual discrepancies which could be the hint of the presence of some BSM physics.

The basic idea of the MC simulation consists in using a random number generator in order to simulate as many events as computationally possible for all the SM processes, taking into account the probability density functions of the process being considered. This is performed by specific softwares called *event generators* and, of course, it is important to note that the perfect event generator does not exist, since we usually don't know everything about the SM or BSM process being generated.

The structure of a pp collision at the LHC as built up by event generators can actually be described by a few main steps that will now be described one by one, as shown in Figure 2.1. The interaction between the particles produced and the detector itself is then usually modeled using standard packages such as GEANT4 [100], able to completely describe this interaction or DELPHES 3 [101], able to provide a fast, yet approximate, simulation of a multipurpose detector.

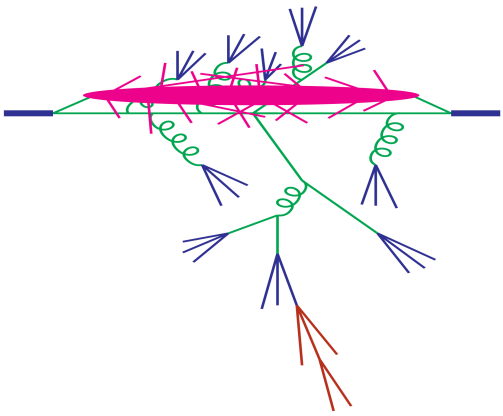

Figure 2.1: Structure of a pp collision and different steps of the MC simulation by the event generators, such as the parton shower (in green), the Underlying Event (UE) (in pink), the hadronization (in blue) and the decay of unstable particles (in red) [102].

Hard scattering

Many processes of interest and expected to be produced by the LHC involve large momentum transfers, such as the production of jets with high transverse momenta or heavy particles. The simulation of such momenta transfers is therefore at the heart of the event generation and is usually referred to as the hard scattering process, the highest momentum transfer process in the event, whose probability distribution can be calculated using perturbation theory and several parameters, such as:

- The Parton Density Functions (PDFs) $f_i(x, Q^2)$ of both partons involved in the collision, giving the probability of finding in the proton a parton of flavor i (quark or gluon) carrying a fraction x of the proton momentum with Q being the energy scale of the hard interaction [103]. Being universal, in the sense that the same PDFs enter in all the processes involving a given hadron, their main parameters are usually determined experimentally from hard-scattering data [104]. They are the key ingredient of the QCD parton model.
- The hard scattering matrix elements squared $|\mathcal{M}_{pp\to n}|^2$, usually evaluated considering all the Feynman diagrams of a given process, where n is the number of outgoing particles.

Many algorithms are then able to read such input parameters in order to compute the parton level cross section using different methods. The samples used in this work have actually been produced at different orders and by different hard scattering generators, such as MADGRAPH [105] (at Leading Order (LO)), POWHEG [106] and MC@NLO [107].

Parton shower

The parton shower phase is used to describe what happens to the incoming and outgoing partons involved in the actual collision.

Hadronization

Underlying Event (UE)

Unstable particle decays

GEANT

nanoAOD

2.2 Data samples

2.3 Signal samples

2.4 Background prediction

2.4.1 The main background: $t\bar{t}$

2.4.2 Drell-Yan estimation

2.4.3 Non prompt contamination

2.4.4 Smaller backgrounds

2.4.5 Weights and corrections applied

Chapter 3

Event selection

3.1 Signal regions

3.2 Control regions

3.3 Background-signal discrimination

3.3.1 Discriminating variables

Missing Transverse Energy (MET)

MT2

3.3.2 Neural network

Chapter 4

Results and interpretations

4.1 Systematics and uncertainties

4.2 Results

Chapter 5

Conclusions

5.1 Future prospects

Appendices

List of figures

List of tables

Bibliography

[1] F. Englert and R. Brout, "Broken symmetry and the mass of gauge vector mesons", Phys. Rev. Lett. 13, pp. 321-323, 1964

[2] P. W. Higgs, "Broken symmetries and the masses of gauge bosons", Phys. Rev. Lett. 13, pp. 508-509, 1964

[3] S. Chatrchyan et al., "Observation of a new boson at a mass of 125 GeV with the CMS experiment at the LHC", Phys. Lett. B716, pp. 30-61, 2012 [arXiv: 1207.7235]

[4] G. Aad et al., "Observation of a new particle in the search for the Standard Model Higgs boson with the ATLAS detector at the LHC", Phys. Lett. B716, pp. 1-29, 2012 [arXiv: 1207.7214]

[5] V.C. Rubin, W.K. Ford and N. Thonnard, "Rotational properties of 21 SC galaxies with a large range of luminosities and radii, from NGC 4605 (R=4kpc) to UGC 2885 (R=122kpc)", Astrophysical Journal 238, pp. 471-487, 1980

[6] K.G. Begeman, A.H. Broeils and R.H. Sanders, "Extended rotation curves of spiral galaxies - Dark haloes and modified dynamics", Monthly Notices of the Royal Astronomical Society, vol. 249, issue 3, ISSN 0035-8711, 1991

[7] A. Robertson, R. Massey and V. EkCMBTemperaturee, "What does the Bullet Cluster tell us about self-interacting dark matter?", Monthly Notices of the Royal Astronomical Society, vol. 465, issue 1, 2017 [arXiv: 1605.04307]

[8] J.B. Mu?oz, C. Dvorkin and A. Loeb, "21-cm Fluctuations from Charged Dark Matter", Phys. Rev. Lett. 121, 121301 (2018) [arXiv: 1804.01092]

[9] A. Natarajan, "A closer look at CMB constraints on WIMP dark matter", Phys. Rev. D85, 2012 [arXiv:1201.3939]

[10] G. D'Ambrosio G.F. Giudice, G. Isidori and A. Strumia, "Minimal Flavour Violation: an effective field theory approach", Nucl.Phys. 645, pp 155-187, 2002 [arXiv:0207.036]

[11] CMS Collaboration, "Search for the production of dark matter in association with top-quark pairs in the single-lepton final state in proton-proton collisions at $\sqrt{s} = 8$ TeV", JHEP, vol. 6 121, 2015

[12] CMS Collaboration,, "Search for the Production of Dark Matter in Association with Top Quark Pairs in the Di-lepton Final State in pp collisions at $\sqrt{s} = 8$ TeV", CMS-PAS-B2G-13-004, 2014

[13] "Search for dark matter in events with heavy quarks and missing transverse momentum in pp collisions with the ATLAS detector", Eur. Phys. J. C (2015) 75:92

[14] ATLAS Collaboration, Search for the Supersymmetric Partner of the Top Quark in the Jets+Emiss Final State at $\sqrt{s} = 13$ TeV", ATLAS-CONF-2016-077

[15] ATLAS Collaboration, "Search for top squarks in final states with one isolated lepton, jets, and missing transverse momentum in $\sqrt{s} = 13$ TeV pp collisions with the ATLAS detector", ATLAS-CONF-2016-050, 2016

[16] ATLAS Collaboration, "Search for direct top squark pair production and dark matter production in final states with two leptons in $\sqrt{s} = 13$ TeV pp collisions using 13.3 fb^{-1} of ATLAS data", ATLAS-CONF-2016-076, 2016

[17] ATLAS Collaboration, "Search for dark matter produced in association with bottom or top quarks in $\sqrt{s} = 13$ TeV pp collisions with the ATLAS detector", Eur. Phys. J. C 78 (2018) 18 [arXiv: 1710.11412]

[18] CMS Collaboration, Search for dark matter produced in association with heavy-flavor quark pairs in proton-proton collisions at $\sqrt{s} = 13$ TeV", Eur. Phys. J. C (2017) 77: 845

[19] CMS Collaboration, "Search for dark matter particles produced in association with a top quark pair at $\sqrt{s} = 13$ TeV", Phys. Rev. Lett. 122, 011803 (2019) [arXiv: 1807.06522]

[20] CMS Collaboration, "Search for dark matter produced in association with a single top quark or a top quark pair in proton-proton collisions at $\sqrt{s} = 13$ TeV", JHEP, vol. 03 141, 2019 [arXiv: 1901.01553]

[21] S. Manzoni, "The Standard Model and the Higgs Boson", Physics with Photons Using the ATLAS Run 2 Data, Springer Theses, 2019

[22] A.B. Balantekin, A. Gouvea and B.Kayser, "Addressing the Majorana vs. Dirac Question with Neutrino Decays", FERMILAB-PUB-18-418-T, NUHEP-TH/18-09 [arXiv: 1808.10518]

[23] J. Woithe, G.J. Wiener and F. Van der Vecken, "Let's have a coffee with the Standard Model of particle physics!", Physics education 52, number 3, 2017

[24] F. Zwicky, "Die Rotverschiebung von extragalaktischen Nebeln", Helvetica Physica Acta , vol. 6, pp. 110-127, 1933

[25] S. Van den Bergh,Phys Rev D "The early history of dark matter", Dominion Astrophysical Observatory, 1999

[26] V.C. Rubin, W.K. Ford, "Rotation of the Andromeda Nebula from a Spectroscopic Survey of Emission Regions", Astrophysical Journal 159, p. 379, 1970

[27] A. A. Penzias, R.W. Wilson, "A Measurement of Excess Antenna Temperature at 4080 Mc/s", Astrophysical Journal 142, pp. 419-421

[28] D.J. Fixsen, "The temperature of the cosmic microwave background", Astrophysical Journal, 2009

[29] Planck Collaboration, "Planck 2018 results. I. Overview and the cosmological legacy of Planck", 2018 [arXiv: 1807.06205]

[30] R. Tojeiro, "Understanding the Cosmic Microwave Background Temperature Power Spectrum", 2006

[31] Planck Collaboration, "Planck 2018 results. VI. Cosmological parameters", 2018 [arXiv: 1807.06209]

[32] "Astrophysical Constants and Parameters", 2019

[33] D. Clowe et all., "A Direct Empirical Proof of the Existence of Dark Matter", Astrophysical Journal Letters 648, 2006

[34] K.R. Dienes, J. Fennick, J. Kumar, B. Thomas "Dynamical Dark Matter from Thermal Freeze-Out", Phys. Rev. D 97, 063522 (2018) [arXiv: 1712.09919]

[35] C.S. Frenk, S.D.M. White, "Dark matter and cosmic structure", Annalen der Physik, p. 22 , 2012 [arXiv: 1210.0544]

[36] R. Kirk, "Dark matter genesis"

[37] M. Drewes et all., "A White Paper on keV Sterile Neutrino Dark Matter", 2016 [arXiv: 1602.04816]

[38] C. Alcock et all., "The MACHO Project: Microlensing Results from 5.7 Years of LMC Observations", Astrophys.J. 542 (2000) 281-307

[39] P. Tisserand et all., "Limits on the Macho content of the Galactic Halo from the EROS-2 Survey of the Magellanic Clouds", A & A 469, pp. 387-404 (2007)

[40] EROS and MACHO collaborations, "EROS and MACHO Combined Limits on Planetary Mass Dark Matter in the Galactic Halo", 1998

[41] Particle Data Group, "Neutrino Cross Section Measurements", PDG 2019

[42] K. McFarland, "Neutrino Interactions", 2008 [arXiv: 0804.3899]

[43] E. Morgante, "Aspects of WIMP Dark Matter Searches at Colliders and Other Probes", Springer theses, 2016

[44] F. Couchot et all., "Cosmological constraints on the neutrino mass including systematic uncertainties", A & A 606, A104 (2017)

[45] E. Bulbul et all., "Detection of An Unidentified Emission Line in the Stacked X-ray spectrum of Galaxy Clusters", 2014 [arXiv: 1402.2301]

[46] A. Boyarsky et all., "An unidentified line in X-ray spectra of the Andromeda galaxy and Perseus galaxy cluster", Phys. Rev. Lett. 113, 251301 (2014) [arXiv: 1402.4119]

[47] A. Boyarsky et all., "Checking the dark matter origin of 3.53 keV line with the Milky Way center", Phys. Rev. Lett. 115, 161301 (2015) [arXiv: 1408.2503]

[48] T. Jeltema1 and S.Profumo, "Deep XMM Observations of Draco rule out at the 99% Confidence Level a Dark Matter Decay Origin for the 3.5 keV Line", 2015 [arXiv: 1512.01239]

[49] D. Wu, "A Brief Introduction to the Strong CP Problem", Superconducting Super Collider Laboratory, 1991

[50] R.D. Peccei, H.R. Quinn, "CP Conservation in the Presence of Pseudoparticles", Phys. Rev. Lett. 38, 1440, 1977

[51] P.W. Graham et all., "Experimental Searches for the Axion and Axion-like Particles", Annual Review if Nuclear and Particle Science 65, 2015 [arXiv: 1602.00039]

[52] CAST collaboration, "New CAST limit on the axion-photon interaction", Nature Physics 13, pp. 584-590 (2017)

[53] B. Penning, "The Pursuit of Dark Matter at Colliders - An Overview", 2017 [arXiv: 1712.01391]

[54] M. Schumann, "Direct Detection of WIMP Dark Matter: Concepts and Status", J. Phys. G46 (2019) no.10, 103003 [arXiv: 1903.03026]

[55] S.C. Martin et all., "The RAVE survey: constraining the local Galactic escape speed", Mon.Not.Roy.Astron.Soc.379:755-772, 2007

[56] K. Freese, M. Lisanti, C. Savage, "Annual Modulation of Dark Matter: A Review", [arXiv: 1209.3339v3]

[57] T.M. Undagoitia and L. Rauch, "Dark matter direct-detection experiments", J. Phys. G43 (2016) no.1, 013001 [arXiv: 1509.08767]

[58] R. Bernabei et all., "First results from DAMA/LIBRA and the combined results with DAMA/NaI", Eur.Phys.J.C56:333-355, 2008 [arXiv: 0804.2741]

[59] J.M. Gaskins, "A review of indirect searches for particle dark matter", Contemporary Physics, 2016 [arXiv: 1604.00014]

[60] F.S. Queiroz, "Dark Matter Overview: Collider, Direct and Indirect Detection Searches", Max-Planck Institute of Physics

[61] LAT collaboration, "Constraints on Dark Matter Annihilation in Clusters of Galaxies with the Fermi Large Area Telescope", JCAP 05(2010)025 [arXiv: 1002.2239]

[62] A.A. Moiseev et all., "Dark Matter Search Perspectives with GAMMA-400", 2013 [arXiv: 1307.2345]

[63] L. Covi et all., "Neutrino Signals from Dark Matter Decay", JCAP 1004:017, 2010 [arXiv: 0912.3521]

[64] B. Lu and H. Zong, "Limits on the Dark Matter from AMS-02 antiproton and positron fraction data", Phys. Rev. D 93, 103517 (2016) [arXiv: 1510.04032]

[65] J. Abdallah et all., "Simplified Models for Dark Matter Searches at the LHC", Phys. Dark Univ. 9-10 (2015) 8-23 [arXiv: 1506.03116]

[66] H. An, L. Wang, H. Zhang, "Dark matter with t-channel mediator: a simple step beyond contact interaction", Phys. Rev. D 89, 115014 (2014) [arXiv: 1308.0592]

[67] ATLAS Collaboration, "Search for dark matter and other new phenomena in events with an energetic jet and large missing transverse momentum using the ATLAS detector", JHEP 01 (2018) 126 [arXiv: 1711.03301]

[68] CMS Collaboration, "Search for new physics in the monophoton final state in proton-proton collisions at $\sqrt{s} = 13$ TeV", J. High Energy Phys. 10 (2017) 073 [arXiv: 1706.03794]

[69] CMS Collaboration, "Search for dark matter produced with an energetic jet or a hadronically decaying W or Z boson at $\sqrt{s} = 13$ TeV", JHEP 07 (2017) 014 [arXiv: 1703.01651]

[70] CMS Collaboration, "Search for new physics in final states with an energetic jet or a hadronically decaying W or Z boson and transverse momentum imbalance at $\sqrt{s} = 13$ TeV", Phys. Rev. D 97, 092005 (2018) [arXiv: 1712.02345]

[71] ATLAS Collaboration, "Search for dark matter in association with a Higgs boson decaying to two photons at $\sqrt{s} = 13$ TeV with the ATLAS detector", Phys. Rev. D 96 (2017) 112004 [arXiv: 1706.03948]

[72] CMS Collaboration, "Search for associated production of dark matter with a Higgs boson decaying to $b\bar{b}$ or $\gamma\gamma$ at $\sqrt{s} = 13$ TeV", JHEP 10 (2017) 180 [arXiv: 1703.05236]

[73] Atlas Collaboration, "Search for new phenomena in dijet events using 37 fb$^{?1}$ of pp collision data collected at $\sqrt{s} = 13$ TeV with the ATLAS detector", Phys. Rev. D 96, 052004 (2017) [arXiv: 1703.09127]

[74] CMS Collaboration, "Search for narrow and broad dijet resonances in proton-proton collisions at $\sqrt{s} = 13$ TeV and constraints on dark matter mediators and other new particles", JHEP 08 (2018) 130 [arXiv: 1806.00843]

[75] C. Munoz, "Models of Supersymmetry for Dark Matter", FTUAM 17/2, IFT-UAM/CSIC-17-005, 2017 [arXiv: 1701.05259]

[76] CMS Collaboration, "Searches for invisible decays of the Higgs boson in pp collisions at $sqrts = 7$, 8, and 13 TeV", JHEP 02 (2017) 135 [arXiv: 1610.09218]

[77] J. Alimena et all., "Searching for long-lived particles beyond the Standard Model at the Large Hadron Collider", 2019 [arXiv: 1903.04497]

[78] A. Albert et all., "Recommendations of the LHC Dark Matter Working Group: Comparing LHC searches for heavy mediators of dark matter production in visible and invisible decay channels", 2017 [arXiv: 1703.05703]

[79] M. Tanabashi et al., Particle Data Group, Phys. Rev. D98, 030001 (2018)

[80] R. Schicker, "The ALICE detector at LHC", 2005

[81] LHCb Collaboration, "LHCb Detector Performance", Int. J. Mod. Phys. A 30, 1530022 (2015) [arXiv: 1412.6352]

[82] E. Gschwendtner, "AWAKE, A Particle-driven Plasma Wakefield Acceleration Experiment", CERN Yellow Report CERN 2016-001, pp.271-288 [arXiv: 1705.10573]

[83] M. Thomson, "Modern Particle Physics", Cambridge University Press, 2013

[84] G. Apollinari et all., "High Luminosity Large Hadron Collider HL-LHC", CERN Yellow Report CERN-2015-005, pp.1-19 [arXiv: 1705.08830]

[85] CMS Collaboration, "The CMS experiment at the CERN LHC", JINST 3 (2008) S08004

[86] CMS Collaboration, "Precision measurement of the structure of the CMS inner tracking system using nuclear interactions", JINST 13 (2018) P10034 [arXiv: 1807.03289]

[87] M.S. Kim, "CMS reconstruction improvement for the muon tracking by the RPC chambers", 2013 JINST 8 T03001 [arXiv: 1209.2646]

[88] CMS Collaboration, "Performance of the CMS muon detector and muon reconstruction with proton-proton collisions at $\sqrt{s} = 13$ TeV", JINST 13 (2018) P06015 [arXiv: 1804.04528]

[89] CMS Collaboration, "Particle-Flow Event Reconstruction in CMS and Performance for Jets, Taus, and MET", CMS-PAS-PFT-09-001, 2009

[90] CMS Collaboration, "Description and performance of track and primary-vertex reconstruction with the CMS tracker", JINST 9 (2014) P10009 [arXiv: 1405.6569]

[91] V. Knunz, "Measurement of Quarkonium Polarization to Probe QCD at the LHC", Springer theses, 2015

[92] CMS Collaboration, "Performance of electron reconstruction and selection with the CMS detector in proton-proton collisions at $\sqrt{s} = 8$ TeV", JINST 10 (2015) P06005 [arXiv: 1502.02701]

[93] J. Rembser, "CMS Electron and Photon Performance at 13 TeV", J. Phys. Conf. Ser. 1162 012008, 2019

[94] P.L.S. Connor, "Review of jet reconstruction algorithms", Ryan Atkin J. Phys. Conf. Ser. 645 012008, 2015

[95] CMS Collaboration, "Jet energy scale and resolution in the CMS experiment in pp collisions at 8 TeV", JINST 12 (2017) P02014 [arXiv: 1607.03663]

[96] F. Beaudette, "The CMS Particle Flow Algorithm", 2014 [arXiv: 1401.8155]

[97] CMS Collaboration, "Identification of heavy-flavour jets with the CMS detector in pp collisions at 13 TeV", JINST 13 (2018) P05011 [arXiv: 1712.07158]

[98] CMS Collaboration, "Performance of missing transverse momentum reconstruction in proton-proton collisions at $\sqrt{s} = 13$ TeV using the CMS detector", JINST 14 (2019) P07004 [arXiv: 1903.06078

[99] L. Sonnenschein, "Analytical solution of ttbar dilepton equations", Phys.Rev.D73:054015, 2016

[100] V. Lefebure and S. Banerjee, "CMS Simulation Software Using Geant4", CMS-NOTE-1999-072, 1999

[101] DELPHES 3 Collaboration, "DELPHES 3, A modular framework for fast simulation of a generic collider experiment", JHEP 1402 (2014) 057 [arXiv:1307.6346

[102] M.H. Seymour and M. Marx, "Monte Carlo Event Generators", MCnet-13-05, 2013 [arXiv:1304.6677]

[103] R. Placakyte, "Parton Distribution Functions", 2011 [arXiv:1111.5452]

[104] L. Del Debbio, "Parton distributions in the LHC era", The European Physical Journal Conferences 175(394), 2018

[105] J. Alwall et all., "MadGraph 5 : Going Beyond", 2011 [arXiv:1106.0522]

[106] C. Oleari, "The POWHEG-BOX", Nucl.Phys.Proc.Suppl.205-206:36-41 [arXiv:1007.3893]

[107] S. Frixione et all., "The MC@NLO 4.0 Event Generator", CERN-TH/2010-216 [arXiv:1010.0819]